Agricultural and Forest Meteorology 354 (2024) 110076

Contents lists available at ScienceDirect

Agricultural and Forest Meteorology

journal homepage: www.elsevier.com/locate/agrformet

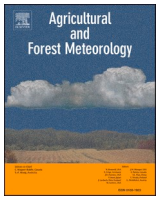

The impact of spongy moth (*Lymantria dispar dispar*) defoliation on carbon balance of a temperate deciduous forest in North America

Lejla Latifovic, M. Altaf Arain *

School of Earth, Environment and Society and McMaster Centre for Climate Change, McMaster University, Hamilton, Ontario, Canada

ARTICLE INFO

Keywords:
Spongy moth
LDD moth (Lymantria dispar dispar)
Natural disturbance
Temperate forest
Carbon cycle
Net ecosystem productivity
Eddy covariance

ABSTRACT

Temperate deciduous forests are an important contributor to the global carbon (C) sink. However, changes in environmental conditions and natural disturbances such as insect infestations can impact carbon sequestration capabilities of these forests. While, insect infestations are expected to increase in warmer future climates, there is a lack of knowledge on the quantitative impact of these natural disturbances on the carbon balance of temperate deciduous forests. In 2021, a record-breaking defoliation, caused by the spongy moth (*Lymantria dispar dispar* (LDD), formerly knows as the gypsy moth) occurred in eastern North America. In this study, we assess the impact of this spongy moth defoliation on carbon uptake in a mature oak-dominated temperate forest in the Great Lakes region in Canada, using eddy covariance flux data from 2012 to 2022. Study results showed that the forest was a large C sink with mean annual net ecosystem productivity (NEP) of 207 ± 77 g C m^{-2} yr^{-1} from 2012 to 2022, excluding 2021, which experienced the infestation. Over this period mean annual gross ecosystem productivity (GEP) was 1,398 ± 137 g C m^{-2} yr^{-1}, while ecosystem respiration (RE) was 1,209 ± 139 g C m^{-2} yr^{-1}. However, in 2021 due to defoliation in the early growing season, annual GEP of the forest declined to 959 g C m^{-2} yr^{-1}, while annual RE increased to 1,345 g C m^{-2} yr^{-1} causing the forest to become a large source of C with annual NEP of -351 g C m^{-2} yr^{-1}. The forest showed a rapid recovery from this major disturbance event, with annual GEP, RE, and NEP values of 1,671, 1,287, and 298 g C m^{-2} yr^{-1}, respectively in 2022 indicating that the forest was once again a large C sink. This study demonstrates that major transient natural disturbances under changing climate can have a significant impact on forest C dynamics. The extent to which North American temperate forests will remain a major C sink will depend on the severity and intensity of these disturbance events and the rate of recovery of forests following disturbances.

Lay abstract: Temperate deciduous forests play an important role in carbon sequestration from the atmosphere. However, the impact of climate change, extreme weather, and disturbance events can alter the extent to which these forests sequester carbon, in some cases shifting their role from being a carbon sink to becoming a carbon source to the atmosphere. In 2021, a spongy moth infestation severely defoliated a mature oak-dominated temperate forest north of Lake Erie, Ontario, Canada, turning the forest from a 10-year mean carbon sink of about 2 tons of carbon per hectare to a carbon source of about 3.5 tons of carbon per hectare. Our analysis indicates that meteorological conditions during the early growing season might have influenced the severity of this infestation. Specifically, the prevalence of dry and warm weather conditions enabled the moth to survive and thrive longer. This study shows the significant influence of natural disturbances on forest carbon dynamics as temperatures continue to rise due to climate change. The future role forests play in carbon sequestration will be determined by the severity of disturbance events and the effectiveness of forests to recover in the aftermath of these events.

1. Introduction

Forests play an important role in global efforts to sequester atmospheric CO_2 and mitigate the impacts of climate warming (Canadell and Schulze, 2014; Keenan and Williams, 2018; Waring et al., 2020). Temperate forests which constitute 25 % (~10.4 million km^2) of the global forest cover, primarily in eastern North America, Europe, and Asia account for up to 37 % of the global forest C uptake (IPCC, 2014;

* Corresponding author at: School of Earth, Environment and Society, McMaster University, 1280 Main Street West, Hamilton, ON, Canada, L8S 4K1.
E-mail address: arainm@mcmaster.ca (M.A. Arain).

https://doi.org/10.1016/j.agrformet.2024.110076
Received 11 July 2023; Received in revised form 12 May 2024; Accepted 16 May 2024
Available online 1 June 2024

Pan et al., 2011; Tyrrell et al., 2012; Monson, 2014). In a recent study, Harris et al. (2021) reported that net C sequestration of temperate forests is approximately 3.6 $GtCO_2e\ yr^{-1}$ (~0.98 GtC or PgC) which is equivalent to offsetting 47 % of forest related GHG emissions or 8.6 % of total global GHG emissions of 42.0 $GtCO_2e\ yr^{-1}$. Most of the temperate forests are deciduous stands, which cover 7.8 million km^2 of land area across the world (Allaby, 2006; Vasseur, 2012), with 2.6 million km^2 of these forests located in eastern North America (Commission for Environmental Cooperation, 2006). Globally, these forests have sequestered 0.72 PgC yr^{-1} from 1990 to 2007 (Pan et al., 2011). However, recent studies indicate that climate change, extreme weather events, and natural and human disturbances are adversely impacting the growth and carbon uptake capabilities of temperate deciduous forests (Beamesderfer, 2020; Dale et al., 2001; Hicke et al., 2012; Hurteau, 2021; Li et al., 2023; Reinmann et al., 2019). There is strong evidence of more frequent and intense insect infestations due to climate change (Ammunét et al., 2012; Hicke et al., 2012; Williams et al., 2016). Because of warmer winter and summer temperatures and changes in precipitation, natural controls on insect outbreaks are being weakened. These include (i) reduced effectiveness of pathogens and viruses due to dry conditions (Hajek et al., 1996), (ii) increase in herbivory as foliage with higher carbon/nitrogen (C:N) ratio is nutritionally poorer and insects are compelled to consume more (Currano et al., 2008; Lindroth et al., 1997), and (iii) shifts in the range of infestation area, where natural controls may not be effective (Régnière et al., 2009; Dale et al., 2001). These more frequent and/or intense infestations result in strong reductions in forest C uptake (Clark et al., 2009; 2018; 2022; Cook et al., 2008; Stephens et al., 2018). They have the potential to cause long-term shifts in forest C dynamics due to tree mortality and the introduction of large amounts of coarse woody debris to forest floors impacting ecosystem respiration (RE) and often transforming a forest from a consistent C sink to a rapid C source (Clark et al., 2009; 2018).

Large tracts of forests in western North America in USA and Canada have been infested with mountain pine beetle with serious implications for forest growth, wood production, and C sequestration (Hicke et al., 2013; Speckman et al., 2015, 2020; Kurz et al., 2008). It was perceived that perhaps eastern North American forests are less impacted by insect infestation, although there was some evidence of mountain pine beetle spreading eastward (Cullingham et al., 2011; Sambaraju et al., 2019). However, in 2021 eastern North American deciduous forests experienced a record-breaking insect infestation by the spongy moth (*Lymantria dispar dispar* (LDD) (Linnaeus, 1758), formerly known as European gypsy moth) that moderately to severely defoliated 1.8 million ha of forest in Southern Ontario, Canada alone (Ontario Ministry of Northern Development, Mines, Natural Resources and Forestry, 2021; Hussain et al., 2024). This infestation was a progression from previous years where a similar infestation in Ontario in 2019 and 2020 impacted 41,600 ha and 569,000 ha of forest, respectively (Ontario Ministry of Northern Development, Mines, Natural Resources and Forestry, 2021). Spongy moth outbreaks are cyclical, occurring every five to ten years (Ward et al., 2022). Previous outbreaks in Ontario occurred in 1985, 1991, 2002, and 2008; however, none reached the intensity of the 2021 outbreak (Ontario Ministry of Northern Development, Mines, Natural Resources and Forestry, 2021). The widespread defoliation in 2021 was also reported in northeastern USA impacting 1.05 million ha forest area with roughly half (0.52 million ha) located in Michigan State (USDA, 2022).

Spongy moth is an invasive species in North America (Liebhold et al., 1992). Introduced accidentally in 1868 or 1869 by an entomologist in Medford, Massachusetts, USA, it has spread to most of the northeastern states in the USA and eastern provinces in Canada (Leroy et al., 2021; Liebhold et al., 1992). Due to its ability to survive by feeding on a wide variety of deciduous tree species such as Oak, Aspen, Basswood, Maple, Willow, Hawthorn, Apple, Birch, Alder, and many others (USDA, 2022), and a warmer, more hospitable climate, it is likely that the population will continue to spread across most of the USA and Canada (Régnière et al., 2009). The moth is an early spring defoliator where early growing season climatic conditions, particularly temperature and moisture, play a key role in the survival, duration, and intensity of the infestation (Barbosa et al., 1983; Leonard, 1981; Liebhold et al., 1992). Some studies suggested that early spring drought conditions contribute to increase the length and intensity of the infestation (Addy et al., 2018; Hajek et al., 1996). Overall spongy moth infestations last for about six weeks (and have been recorded for up to ten weeks) but with devastating consequences for tree foliage, health, and long-term survival of the trees (Leroy et al., 2021; Ward et al., 2022). Given that climate in eastern North America is expected to become warmer and dryer (Arain et al., 2022), it is reasonable to expect the persistence of insect infestations in the future. Therefore, it is increasingly important to examine how northern temperate forests will respond to these infestations and what are underlying mechanisms that could impact the severity of the infestation and forest C dynamics.

In this study we examined how a spongy moth outbreak early in the growing season in 2021 impacted the C sequestration potential of a mature deciduous forest in the Great Lakes region of Ontario, Canada. The specific objectives of the study were to **(1)** examine eddy covariance CO_2 fluxes measured in this deciduous forest over an eleven-year (2012–2022) period, including spongy moth infestation year of 2021, **(2)** determine the impact of the spongy moth outbreak on net ecosystem productivity (NEP) of the forest, and **(3)** investigate how photosynthesis and ecosystem respiration fluxes might have contributed to changes in NEP of the forest during the infestation by comparing pre- and post-infestation fluxes.

2. Methods

2.1. Study site

The Turkey Point Deciduous (TPD) forest (42°38′7″N, 80° 33′28″W; 265 m above sea level) is a ~90-year-old forest of the Turkey Point Environmental Observatory (TPEO). TPEO is part of the Global Water Futures (GWF), Global Centres, AmeriFlux, and global FLUXNET networks. In these networks, TPD forest is know as CA-TPD. In addition to TPD or CA-TPD forest, TPEO also includes three different age-sequenced conifer forests (83-, 48-, and 20-year-old as of 2022; know as CA-TP4, CA-TP2 and CA-TP1), and an agriculture site (Ca-TPAg) located north of Lake Erie in Ontario, Canada, (Arain 2022; Arain et al., 2022).

In the early 1900′s the area was transformed by forest clearance for agriculture, reducing forest cover from 90 % to 11 % (Richard and Hewitt, 2008). By mid-19th century reforestation efforts following agriculture abandonment increased forest cover to about 19 % (Richard and Hewitt, 2008). Trees at TPD site (75-to-115-year old range) have a mean tree height of 25.7 ± 7.44 m. The forest was naturally regenerated on sandy plains or abandoned agricultural lands, and is located in the Lake Erie-Lake Ontario Ecoregion 7E (Crins et al., 2009). This is the most southern forest ecoregion in Ontario and Canada and is home to Canada's largest remaining Carolinian forests (Crins et al., 2009). At TPD site, the dominant tree species is white oak (*Quercus alba*), and secondary species include red oak (*Quercus rubra*), black oak (*Quercus velutina*), sugar maple (*Acer saccharum*), red maple (*Acer rubrum*), American beech (*Fagus grandifolia*), yellow birch (*Betula alleghaniensis*), white ash (*Fraxinus americana*), and some (roughly 5–10 % of trees) conifer species, predominantly white pine (*Pinus strobus*). The understory is composed of a rich diversity of young deciduous trees and plants, including putty root (*Aplectrum hyemale*), yellow mandarin (*Disporum lanuginosum*), Canada mayflower (*Maianthemum canadense*), red trillium (*Trillium erectum*), black cherry (*Prunus serotina*), wood violet (*Viola palmata*), and horsetail (*Equisetum*).

The forest is managed by the Long Point Region Conservation Authority (LPRCA). Prior to 1994 periodic harvesting has taken place in this forest stand. In 1984 and 1986, a commercial harvesting event removed 440 m^3 and 39.97 m^3 of wood volume, respectively. Between

1989 and 1994 harvesting of white pine (106 m^3), red pine (71.42 m^3), poplar (48.22 m^3), and dead oak (61.35 m^3) took place (Beamesderfer et al., 2020).

Soil in the region is predominantly composed of fine-grained sandy glacial deposits with more than 90 % sand content (Richard and Hewitt, 2008). Classified in the Canadian System of Soil Classification as Brunisolic Gray-Brown Luvisol, these soils are well-drained and have low water holding capacity (Presant and Acton, 1984). The topography is relatively flat, and the study site is surrounded by agricultural fields.

The climate of the region is the mildest in Canada with cool winters and hot and humid summers; classified by Ecoregions Working Group (1989) as the Humid High Moderate Temperate Ecoclimate Region (Crins et al., 2009).

2.2. Eddy covariance flux and meteorological measurements

Continuous half-hourly flux measurements of energy, water, and carbon dioxide (CO_2) commenced on January 5, 2012, using a closed-path eddy covariance (EC) system (CPEC) following protocols set forth by Fluxnet-Canada and global FLUXNET (Fluxnet-Canada, 2003). While measurements continue to present day, this paper considers only those obtained by December 31, 2022. The eddy covariance flux observation system is comprised of a LI-7200 enclosed CO2/H2O infrared gas analyzer (IRGA, LI-COR Inc., Lincoln, NE, USA) and CSAT3 3-D Sonic Anemometer (Campbell Scientific Inc., Edmonton, AB, Canada). These sensors are installed on top of a 36 m high walk-up scaffolding tower. Eddy covariance fluxes were measured at 20 Hz and averaged to half-hourly values using a data computer housed within a field trailer at the base of the tower. The IRGA was calibrated for zero and span offsets approximately once a month in the summer and less often in the winter.

CO_2 storage flux, also known as the rate of change in CO_2 concentration in the air column below the EC measurement level (Sco_2) was calculated by observing the difference between current and previous half-hourly CO_2 concentration measurements at two (mid-canopy and top of tower) heights. A second IRGA (LI-820, LI-COR Inc) was used to sample air at mid-canopy at 16 m height. When mid-canopy measurements were not available the CO_2 storage flux was calculated using the above canopy CO_2 concentration measurements only (36 m).

Vertical CO_2 flux (Fc) between forest and the atmosphere was calculated by multiplying the variations in CO_2 mixing ratio (c') and vertical wind velocity (w') (Baldocchi 2003; Baldocchi et al., 2001). Net ecosystem exchange (NEE) was calculated as the sum of carbon flux (Fc) and the rate of CO_2 storage change (ΔSco_2) in the air column below the EC sensors. NEP was considered as the inverse of NEE. Therefore, positive values of NEP indicate carbon sequestration, while negative values indicate carbon loss from the forest to the atmosphere.

Air temperature (Ta) and relative humidity (RH) were measured using the HMP155A Temperature and Relative Humidity Probe (Vaisala Oyj, Helsinki, Finland). For accuracy and protection from solar radiation interference, the probe is housed within a Compact Aspirated Radiation Shield model 43,502-L (R.M. Young Company, Traverse City, MI, USA). Horizontal wind speed and direction were measured using a Wind Monitor model 05,103 (R.M. Young Inc.). Photosynthetically active radiation (PAR), upwards and downwards, was measured using PQS1 PAR Quantum Sensor (Kipp & Zonen Inc., Delft, Netherlands) while the four components of radiation were measured using CNR4 Net Radiometer (Kipp & Zonen Inc). Radiation sensors are installed on a metal boom 2.5 m away from the tower to eliminate interference from the support structure. The above-described instruments are all mounted at the top of the scaffolding tower between 35 and 37 m in height. An additional below canopy PAR sensor (PQS1, Kipp & Zonen Inc.) and a barometric pressure sensor (61,302 V, R.M. Young Inc) measuring atmospheric pressure are installed at the ground. The below canopy PAR sensor measures radiation penetrating the forest canopy at 1.7 m above ground level.

Precipitation (P) data was collected at a location 15 km east of TPD site using an all-weather weighing bucket precipitation gauge (T-200B, GEONOR Inc., Augusta, NJ, USA).

Soil temperature (Ts) and soil moisture (θ) were measured using probes at 2, 5, 10, 20, 50, and 100 cm depths in two different soil locations. Ts was measured using 107 Temperature Probe (Campbell Scientific Inc., Edmonton, AB, Canada) and θ using CS650 Soil Water Content Reflectometer (Campbell Scientific Inc.). All data was recorded using multiple data loggers; model CR3000 for meteorological data and model CR10X for precipitation. Automated half-hourly data downloads were conducted, and data saved to the desktop computer housed in the field trailer. Further details of instrumentation are given in Beamesderfer et al. (2020).

2.3. Data processing and gap-filling

All data was quality controlled using the Biometeorological Analysis, Collection, and Organizational Node (BACON) software following protocols designed by the Fluxnet-Canada and AmeriFlux Network (Brodeur, 2014). Thresholds were set for all variables using standard values and any data outside of these thresholds was discarded. Data was also manually cleaned to remove any erroneous spikes the thresholds did not catch. Within meteorological data, small gaps consisting of a few half-hour periods were linearly interpolated while larger gaps, spanning hours to days, were filled using linear regression model fitted values from other Turkey Point Environmental Observatory sites. The mean flux recovery was 92.5 % (ranging from 80 % to 98 %) over the study period.

The eddy covariance method typically underestimates CO_2 fluxes under calm and stable atmospheric conditions when there is weak turbulent mixing (low friction velocity) such as during calm nights. Distinction between calm and windy conditions was determined using a friction-velocity, u-star threshold (u*) of 0.4 m s^{-1}. Values obtained under this threshold were assumed to be distorted and therefore were rejected and replaced with gap-filling procedures as outlined in Brodeur (2014). Employing this method resulted in a mean data capture of 55 %; with a range between 47 % to 58 % over the study period. Gaps in NEP were filled as the difference in modelled gross ecosystem productivity (GEP) and modelled ecosystem respiration (RE). GEP represents photosynthesis at the ecosystem level (Lovett et al., 2006), while RE is the sum of autotrophic respiration (i.e. C lost to atmosphere due to leaf, stem, and root maintenance and growth respiration) and heterotrophic respiration (i.e. C lost to atmosphere due to decomposition of organic matter). RE was assumed to be equal to nighttime NEE (-NEP) when u* > 0.4 m s^{-1}. These nighttime RE values were used to model a continuous time series of RE based on a non-linear regression with soil temperature, Ts at 5 cm depth and soil moisture θ_{0-30} cm (depth-weighted using measurements at 5, 10, 20, and 50 cm) using the following relationship:

$$RE = R_{10} \times Q_{10}^{\frac{T_s-10}{10}} \times f(\theta_{0-30cm}) \quad (1)$$

where R_{10} and Q_{10} are fitted temperature response parameters that describe the relationship between RE and T_s (Brodeur, 2014). $f(\theta_{0-30cm})$ is a sigmoidal function that characterizes the role of θ_0_30 cm in modifying the temperature response of RE as:

$$f(x) = \frac{1}{[1 + \exp(\theta_1 - \theta_2 x)]} \quad (2)$$

θ_1 and θ_2 are fitted parameters as a function of the independent variable x, in this case θ_0_30 cm, thus acting as a scaling function on the T_s, RE relationship (Brodeur, 2014).

Half-hourly gross ecosystem productivity (GEP) was determined by adding measured NEP to modelled daytime RE. Gaps in GEP were modelled using a rectangular hyperbolic function:

$$GEP = \frac{\alpha PARd\, A_{max}}{\alpha PARd + A_{max}} \times f(T_s) \times f(VPD) \times f(\theta_{0-30cm}) \quad (3)$$

The first term in the equation defines a Michaelis-Menten relationship between PARd (downwelling photosynthetically active radiation) and GEP, where fitted parameter α is the photosynthetic flux per quanta of PARd (quantum yield) and fitted parameter A_{max} is the photosynthetic capacity. For each year A_{max} and α values were calculated by regressing bin-averaged half-hourly GEP and PAR data. Higher values of α and A_{max} are indicative of higher productivity of the forest. $f(T_s)$, $f(VPD)$, and $f(\theta_{0-30cm})$ are sigmoidal-type scaling responses of GEP to soil temperature (Ts), vapour pressure deficit (VPD), and soil moisture (θ_{0-30cm}) (Brodeur, 2014).

For analysis half-hourly NEP estimates were aggregated to daily, monthly, and annual values. Annual values were considered as calendar year. "Hot years" were categorized as the years that had an estimated 30 or more hot days in a given year (Arain et al., 2022). Hot days were defined as days when daily maximum temperature was (T_{max}) $\geq$ 27.5 °C, which is the 90th percentile of daily T_{max} over the 30-year reference period (1971–2000) (Arain et al., 2022). Data processing and analysis was conducted in MATLAB software (The MathWorks Inc., Natick, MA) versions R2019b and R2022b.

2.4. Growing season

In order to estimate the onset and end of the growing season, five-day running daily mean GEP and maximum daily GEP values for a given year were calculated. The onset of the growing season was considered as the first occurrence of five consecutive days when five-day running daily mean GEP exceeded 15 % of the maximum observed daily GEP in a given year (Chan et al., 2018; Coursolle et al., 2012). The end of the growing season was determined as the first occurrence when, over a span of five consecutive days, the running daily mean GEP dropped below 15 % of the maximum value observed throughout the entire year (Chan et al., 2018; Coursolle et al., 2012).

2.5. Estimates of LAI

LAI was estimated using the Simple Method as described by Rogers et al. (2021).

$$Le = -\frac{\cos(\Theta)}{G(\Theta)}\ln(P(\Theta)) \quad (4)$$

Briefly, Eq (4) was applied to half-hourly above and below canopy PAR measurements to determine the Gap Fraction (P) at a specific Solar Zenith Angle (Θ). Using the Simple Method, we assume leaf angle distribution within the canopy is spherical with G(Θ) value of 0.5.

3. Results

3.1. Growing season

The growing season typically begins during the first two weeks of May each year, with the earliest star date recorded on May 1 in 2012 and the latest on May 20 in 2014. In 2022, the growing season lasted the longest at 170 days, while in other years, it ranged between 149 and 168 days (Table 1). During this time GEP typically offsets RE and determines the strength of the forest's annual C sink. The growing season typically ends between October 15 and October 27. Fig. 1

3.2. Meteorological measurements

Over the 11-year study period, mean annual PAR at the site was 291 ± 25 μmol m^{-2} s^{-1}; Ta was 10 ± 1.1 °C; Ts_{5cm} was 9.7 ± 0.6 °C; VPD was 0.4 ± 0.1 kPa; θ_{0-30cm} was 0.11 ± 0.01 m^3 m^{-3}, and P was 1118 ± 256 mm (Table 2). An ongoing trend of slightly increasing PAR over the last three years of the study period (2020 to 2022) was also observed with mean annual PAR surpassing 300 μmol m^{-2} s^{-1} in 2020 (Fig. 2, Table 2). In 2021, there was a distinct deviation from the expected trend in below canopy PAR due to defoliation (Fig. 3), however no noticeable change in reflected PAR was observed (Fig. 2). In the early growing season in 2021, below canopy PAR values followed a typical pattern, remaining slightly below average until early May. However, from the start of June 2021 below canopy PAR rapidly and significantly increased as compared to other years. Below canopy PAR increased from 31 μmol m^{-2} s^{-1} on May 23, 2021, to 128 μmol m^{-2} s^{-1} on June 13, 2021, signifying a more than 300 % rise within 21 days. The rise in below canopy PAR was during a period when canopy rapidly develops to achieve closure. A notable reduction or even the absence of canopy foliage allowed transmission of radiation to the forest floor (Figs. 3 and 2). In comparison to previous years, the peak below canopy PAR value in June 2021 was 140 μmol m^{-2} s^{-1}, while in June 2013, during another year when below canopy PAR reached above average values, peak PAR was 60 μmol m^{-2} s^{-1}. In 2021, below canopy PAR remained high from June to mid-October as well, indicating that canopy had not fully recovered after infestation (Fig. 3).

In addition, estimates of LAI revealed a notable decline in growing season LAI in 2021, particularly during the early growing season (Fig. 4). By June, LAI had decreased to a value below 3 m^2 m^{-2}, which was lower than the 4 to 6 m^2 m^{-2} range observed in all other years over the same period.

During the 11-year study period, the site's mean annual temperature of 10.0 ± 1.1 °C exceeded the 30-year (1991–2020) regional mean temperature of 8.4 °C observed at Environment Canada's Delhi Weather Station (24 km away in the northeast) by 1.6 °C. This increase in Ta also surpassed the average Ta documented at our site by Beamesderfer et al.

Table 1
Growing season (GS) length and number of hot days. The table presents data on the length of the growing season and the number of hot days estimated for each growing season. Hot years, indicated by shading in grey, are defined as years with an estimated 30 or more hot days, identified as having a daily maximum temperature of 27.5 °C or higher. The years considered as hot years in this analysis include 2012, 2016, 2018, 2020, 2021, and 2022.

	2012	2013	2014	2015	2016	2017	2018	2019	2020	2021	2022
GS Start	01-May	07-May	20-May	07-May	17-May	15-May	14-May	19-May	16-May	13-May	10-May
GS End	15-Oct	15-Oct	15-Oct	18-Oct	27-Oct	26-Oct	22-Oct	17-Oct	19-Oct	25-Oct	26-Oct
Length (in days)	168	162	149	165	164	165	162	162	157	166	170
Number of hot days	73	19	8	15	35	20	48	19	40	39	31

Photo A Photo B

Fig. 1. Photos captured at a mature, oak-dominated, deciduous forest part of the Turkey Point Environmental Observatory, north of Lake Erie, Ontario, Canada. Photo A, taken during peak growing season on June 21, 2021, illustrates the extent of defoliation experienced, and Photo B, taken on June 15, 2022 at a near by location, shows the abundance of canopy.

Table 2
Summary statistics for annual (A) and growing seasons (GS) (May to October) meteorological variables. The table presents data on annual photosynthetically active radiation (PAR), air temperature (Ta), soil temperature at 5 cm depth (Ts_{5cm}), vapour pressure deficit (VPD), precipitation (P), and soil moisture (θ_0_30 cm). Mean ± standard deviation values over the study period (2012 to 2022) are also shown. Mean ± standard deviation values excluding 2021 are given in parenthesis.

		2012	2013	2014	2015	2016	2017	2018	2019	2020	2021	2022	Mean ± Std
Mean PAR (μmol m^{-2} s^{-1})	A	287	267	280	285	287	270	266	276	317	321	343	291 ± 25 (288 ± 24)
	GS	394	371	377	382	403	376	369	384	445	421	472	399 ± 33 (397 ± 34)
Mean Ta (°C)	A	11.8	9.2	8.0	9.2	10.6	10.0	9.7	9.1	10.6	11.3	10.3	10.0 ± 1.1 (9.9 ± 1.1)
	GS	19.3	17.5	17.1	17.8	18.8	17.9	19.0	17.8	18.1	19.3	18.8	18.3 ± 0.7 (18.2 ± 0.7)
Mean Ts_{5cm} (°C)	A	10.4	9.2	8.8	9.8	10.7	10.0	9.5	9.2	9.7	10.3	9.6	9.7 ± 0.6 (9.7 ± 0.6)
	GS	16.2	15.8	15.3	15.8	16.3	15.9	16.5	15.8	15.8	16.9	15.7	16 ± 0.4 (15.9 ± 0.3)
Mean VPD (kPa)	A	0.57	0.35	0.33	0.35	0.42	0.36	0.33	0.29	0.37	0.38	0.38	0.4 ± 0.1 (0.4 ± 0.1)
	GS	0.84	0.51	0.49	0.52	0.63	0.52	0.51	0.43	0.54	0.53	0.62	0.56 ± 0.1 (0.56 ± 0.1)
Total P (mm)	A	1001	1266	1429	811	778	1153	1644	1126	1127	1009	960	1119 ± 256 (1130 ± 267)
	GS	607	640	584	500	349	501	864	579	564	681	630	591 ± 127 (582 ± 131)
Mean θ_0_30 cm (m^3 m^{-3})	A	0.10	0.11	0.11	0.10	0.09	0.10	0.11	0.11	0.11	0.12	0.11	0.11 ± 0.01 (0.11 ± 0.01)
	GS	0.08	0.10	0.10	0.09	0.06	0.08	0.09	0.09	0.08	0.11	0.09	0.09 ± 0.01 (0.09 ± 0.01)

(2020) over the initial five-years of measurements (2012 to 2016) by 0.3 °C. In 2021, the annual average Ta reached 11.3 °C, making it the second warmest year during the study period (Table 2). Soil temperatures at 5 cm below ground closely mirrored air temperature. In 2021, mean annual Ts_{5cm} was 10.3 °C, ranking as the third-highest recorded over the 11-year period (Table 2). In 2021, there was a notable increase in VPD during the early part of the year (March) and at the start of the growing season, specifically in May, when daily VPD reached peak value at 1.7 kPa on May 20, 2021 (Fig. 2). Simultaneously, there was a decrease in precipitation, with only 38 mm recorded in May, well below the 11-year

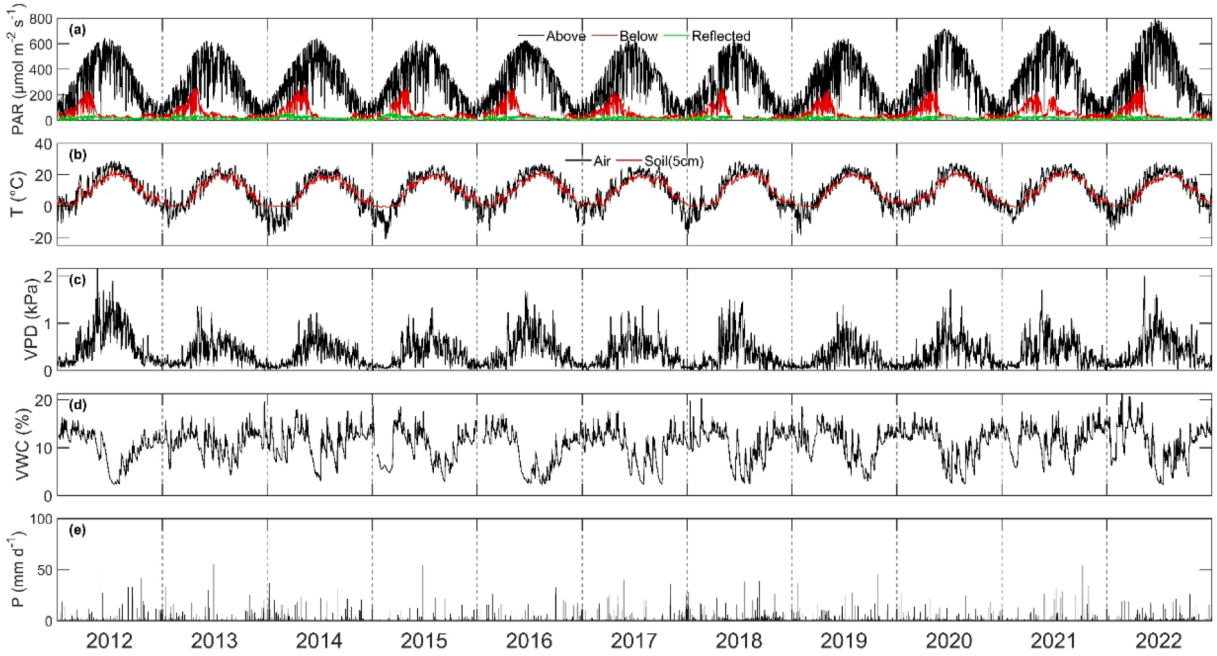

Fig. 2. Daily time series of mean (a) above, below canopy, and reflected photosynthetically active radiation (PAR), (b) air (Ta) and soil temperature at 5 cm depth (Ts), (c) vapor pressure deficit (VPD), (d) soil moisture (VWC), and (e) precipitation (P) at TPD from 2012 to 2022.

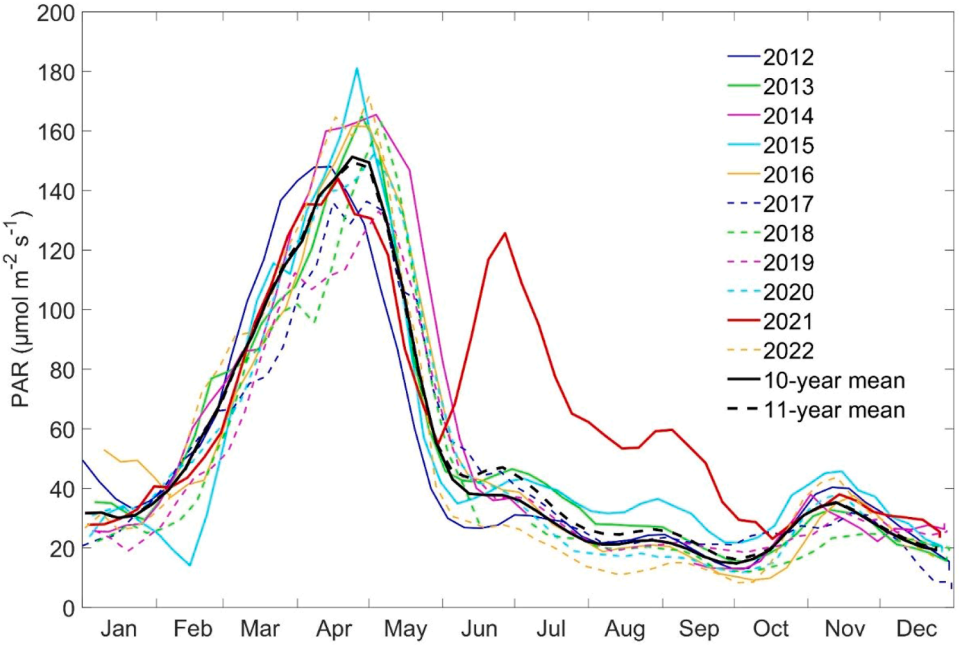

Fig. 3. Mean monthly below canopy photosynthetically active radiation (PAR). The 10-year mean excludes 2021, while the 11-year mean includes all years.

average of 86 mm for the same month. Although annual P value of 1009 mm in 2021 was below average annual P values of 1119 ± 256 mm, a series of steady rainfall events followed the May dry period (Fig. 5). Consequently, mean annual θ_0_30 cm was slightly elevated in 2021, likely due to reduced consumption of soil water by the forest. Overall, in 2021 noticeable differences in meteorological variables occurred, specifically in the early growing season, characterized by warmer and dryer conditions. These changes provided favourable conditions for the hatching, feeding, and growth of spongy moth larvae on foliage.

3.3. Carbon fluxes

Our eddy covariance flux observations showed that the forest was a moderate to strong net C sink on an annual basis (Table 3). Mean annual NEP was 207 ± 77 g C m^{-2} yr^{-1}, GEP was 1398 ± 137 g C m^{-2} yr^{-1}, and RE was 1209 ± 139 g C m^{-2} yr^{-1} from 2012 to 2022, excluding 2021, which experienced an intense infestation of spongy moth causing large scale defoliation of deciduous trees (Table 3). In 2021, GEP declined to 959 g C m^{-2} yr^{-1} and RE increased to 1345 g C m^{-2} yr^{-1} resulting in annual NEP of −351 g C m^{-2} yr^{-1}, which indicated that the infestation had converted the forest into a very large source of C (Table 3). During the 2021 growing season daily GEP exhibited lower values compared to

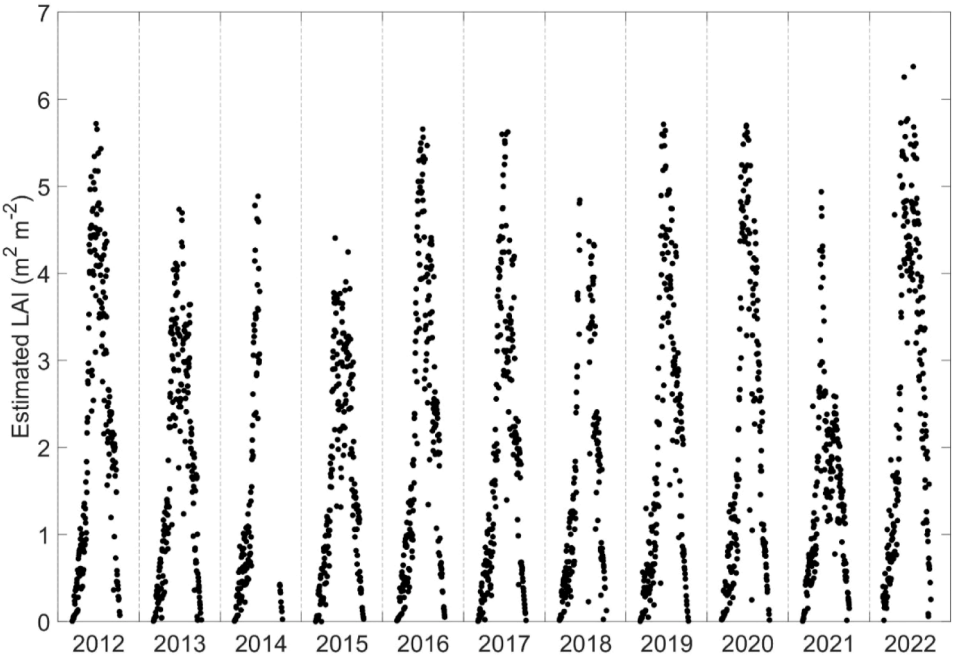

Fig. 4. Daily Leaf Area Index (LAI) estimates for TPD from 2012 to 2022, calculated using the LAI Simple Method as described by Rogers et al. (2021). The plot displays the maximum LAI value for each day.

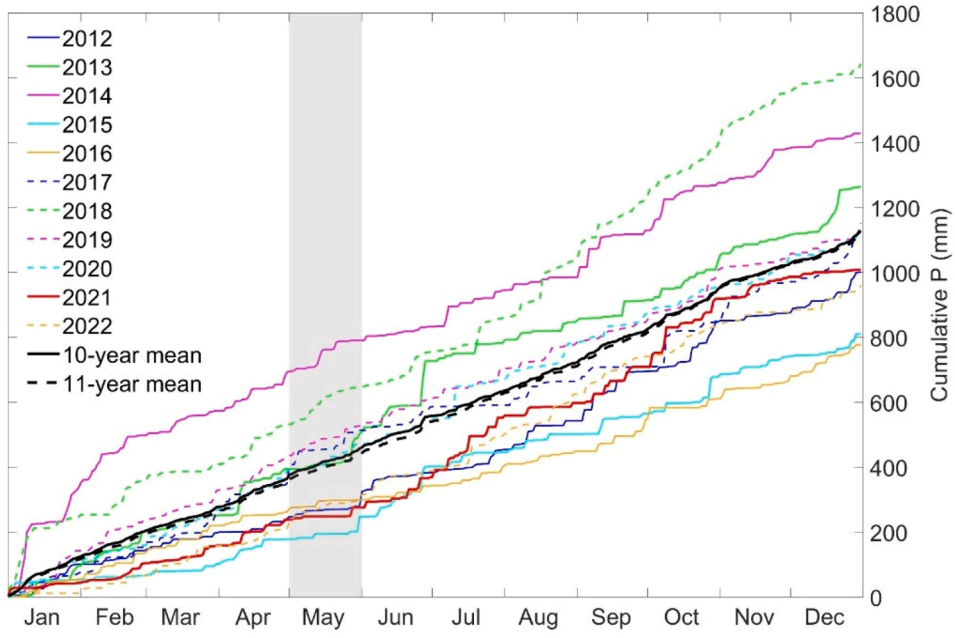

Fig. 5. Daily cumulative precipitation (P) from 2012 to 2022. The 10-year mean excludes 2021, while the 11-year mean includes all years. Grey shading shows early growing season cumulative precipitation levels.

other years (Fig. 6). Mean daily GEP value during June 7 to July 14 (peak infestation) period in 2021 was 5.7 g C m^{-2} d^{-1} while mean daily GEP value over the same period from 2012 to 2020 was 10.3 g C m^{-2} d^{-1}. This difference in GEP (2021 vs 2012–2022) is statistically significant ($p < 0.001$). Although GEP started to recover from mid-July in 2021, values remained low for the remainder of the growing season as compared to non-infestation years (Fig. 6).

A regression analysis between bin-averaged half-hourly PAR and GEP values indicated decreased photosynthetic potential caused by the absence of leaves (Fig. 7). For example, in 2021 at a PAR value of 800 μmol m^{-2} s^{-1}, GEP was only 11.2 μmol m^{-2} s^{-1}, compared to 13.3 to 17.9 μmol m^{-2} s^{-1} for all other years. Moreover, in 2021, quantum yield (α) and maximum photosynthetic capacity (A_{max}) of the forest, were 0.031 mol CO_2 mol^{-1} photons and 20.57 μmol m^{-2} s^{-1}, respectively, which was significantly lower than mean α and A_{max} values of 0.041 mol CO_2 mol^{-1} photons and 32.22 μmol m^{-2} s^{-1}, respectively, over the 2012–2020 period (Table 4).

Daily RE values typically reached peak during the second half of the growing season, anywhere from late July to early September (Fig. 6). However, in 2021, while daily RE values were within the range of interannual variation, peak RE occurred earlier in the summer (by the end of June) and then continued to remain high until middle of August

Table 3
The table presents a summary of annual (A) and growing seasons (GS) (May to October) gross ecosystem productivity (GEP), ecosystem respiration (RE), and net ecosystem productivity (NEP) flux values. Mean ± standard deviation values over the study period (2012 to 2022) are also shown. Mean ± standard deviation values excluding 2021 are given in parenthesis.

		2012	2013	2014	2015	2016	2017	2018	2019	2020	2021	2022	Mean ± Std
GEP (g C m^{-2} yr^{-1})	A	1123	1387	1382	1346	1417	1441	1316	1484	1412	959	1671	1358 ± 186 (1398 ± 137)
	GS	1070	1335	1335	1307	1365	1387	1267	1434	1356	928	1588	1307 ± 176 (1344 ± 130)
RE (g C m^{-2} yr^{-1})	A	860	1279	1120	1282	1250	1316	1144	1250	1306	1345	1287	1222 ± 138 (1209 ± 139)
	GS	599	1049	892	1021	959	1031	913	1000	959	1020	1075	956 ± 131 (950 ± 136)
NEP (g C m^{-2} yr^{-1})	A	310	143	294	89	192	165	189	251	142	−351	298	157 ± 183 (207 ± 77)
	GS	475	286	442	277	402	357	343	428	392	−116	497	344 ± 168 (390 ± 74)

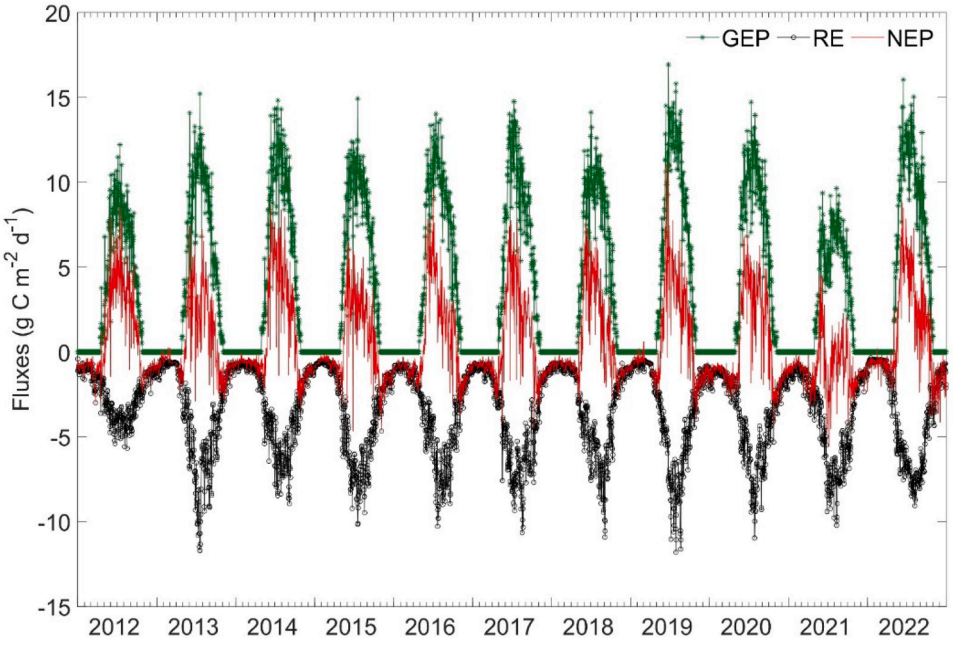

Fig. 6. Daily sum of total gross ecosystem productivity (GEP), ecosystem respiration (RE), and net ecosystem productivity (NEP) from 2012 to 2022.

indicating a change in respiratory flux dynamics of the forest during the infestation year (Fig. 6). However, no significant change in RE was observed in post infestation year, 2022 (Table 3).

In this forest, daily mean NEP values rapidly increase in May after leafout and plateau in June-July at about 6 to 8 g C m^{-2} d^{-1} and then gradually decrease during the second half of the growing season (Fig. 6). However, in 2021, a maximum daily NEP value of 4.5 g C m^{-2} d^{-1} was observed on May 31, followed by a continuous decline in June, reaching the lowest value of −5.57 g C m^{-2} d^{-1} in early July (Fig. 6). By middle of July, as GEP began to increase again due to re-emergence of new leaves and NEP began to slowly recover, NEP only occasionally surpassed 0 g C m^{-2} d^{-1} for the rest of the growing season. Dynamics of cumulative daily NEP values showed that prior to the infestation, the forest became a net C sink (cumulative NEP > 0) between June 12 (2022) to July 3 (2020) (Fig. 8). Then the steady increase in cumulative NEP continued until the end of the growing season. However, early on in 2021, as RE increased before the growing season started and there was no GEP to offset RE, cumulative NEP reached a lower value in April as compared to other years, except in 2020, indicating a larger loss of C to the atmosphere prior to the start of the growing season (Fig. 6). As GEP quickly started to rise following May 10 due to bud break and leaf emergence, there was a small increase in NEP from May to early June but after mid-June, as GEP declined due to the infestation and RE continued to increase, NEP continued to decline for the rest of the year (Fig. 8).

Mean annual GEP, RE, and NEP values over the non-infestation years (2012–2020 and 2022) were 1398 ± 137, 1209 ± 139, and 207 ± 77 g C m^{-2} yr^{-1}, respectively, indicating that the forest was a moderate to strong net C sink. However, after including C flux values of the infestation year, mean annual GEP and NEP values declined to 1358 ± 186 and 157 ± 183 g C m^{-2} yr^{-1}, respectively, while mean annual RE increased to 1222 ± 138 g C m^{-2} yr^{-1} (Table 3, Fig. 6). It shows that the infestation event led to an overall decrease in GEP by 439 g C m^{-2} yr^{-1} (30 %) compared to non-infestation mean annual values. Conversely, RE increased by 136 g C m^{-2} yr^{-1} (11 %) and this contrast between GEP and RE resulted in a total change in NEP of 558 g C m^{-2} yr^{-1}. The forest transformed from being a C sink with mean annual NEP of 207 ± 77 g C m^{-2} yr^{-1} over pre-infestation years, to a large C source, with annual NEP of −351 g C m^{-2} yr^{-1} (270 % reduction) in 2021.

The forest showed a very quick and almost full recovery in the following year. In 2022, annual GEP, RE, and NEP values were 1671, 1287, and 298 g C m^{-2} yr^{-1}, respectively.

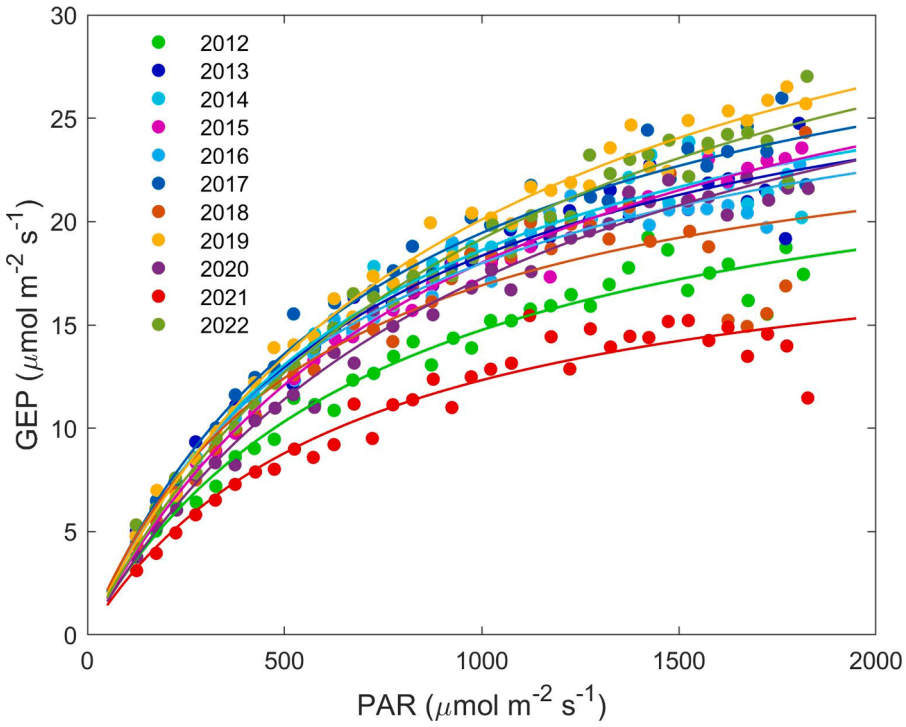

Fig. 7. Non-gapfilled, daytime measurements during the growing season, showcasing bin-averaged half-hourly gross ecosystem productivity (GEP) and bin-averaged photosynthetically active radiation (PAR) levels (bin size: 50 μmol m^{-2} s^{-1}) for 2012 to 2022. The curves represent the fitted hyperbolic model to capture the underlying trend in the data.

Table 4
The relationship between gross ecosystem productivity (GEP) and photosynthetically active radiation (PAR) is illustrated by quantum yield, α (mol CO_2 mol^{-1} photons), maximum photosynthetic capacity, Amax (μmol m^{-2} s^{-1}) and r^2 values fitted onto the best-fit curve. The goodness of fit for each regression is indicated by the coefficient of determination (r^2). The infestation year, 2021 is shaded in grey.

Year	α	A_{max}	r^2
2012	0.035	25.78	0.96
2013	0.044	31.36	0.97
2014	0.044	32.27	0.97
2015	0.037	35.19	0.99
2016	0.045	30.05	0.98
2017	0.045	34.06	0.97
2018	0.047	26.42	0.84
2019	0.041	39.59	0.99
2020	0.034	35.28	0.98
2021	**0.031**	**20.57**	**0.92**
2022	0.038	38.96	0.98
Mean (2012-2020)	**0.041**	**32.22**	**0.96**

4. Discussion

Our forest site and the whole region experienced a massive spongy moth infestation in 2021, most likely due to warm and dry conditions over the winter and into the early growing season, during which no significant rainfall event occurred before late June. Early spring precipitation events usually cause spongy moth larvae that have not yet established feeding sites on foliage to be washed off and die (Leonard, 1981). However, warm and dry early growing season conditions in 2021 created a conducive environment for the growth of spongy moth larvae, allowing them to establish on leaves before the usual late spring rain events in the region. Additionally, warm winter temperatures likely helped spongy moth eggs survive the winter, leading to a more intense infestation. These observations align with findings from the literature, where spongy moth outbreaks have been associated with years of hot and dry weather conditions (Pernek et al., 2008; Leonard, 1981). Specifically, higher temperatures following hatch have been linked to faster growth and development, and increased rates of survival of larvae (Leonard, 1981; Weed et al., 2013). In contrast, low spongy moth populations have been linked to high moisture during early spring (Pernek et al., 2008; Ward et al., 2022). These observations suggest that conducive meteorological conditions during the early growing season at our forest had contributed to increased survival and accelerated development of the larvae thereby intensify the outbreak. What might be of more significance is that prolonged dry conditions may have limited an entomopathogenic fungus' spore germination and the growth of a

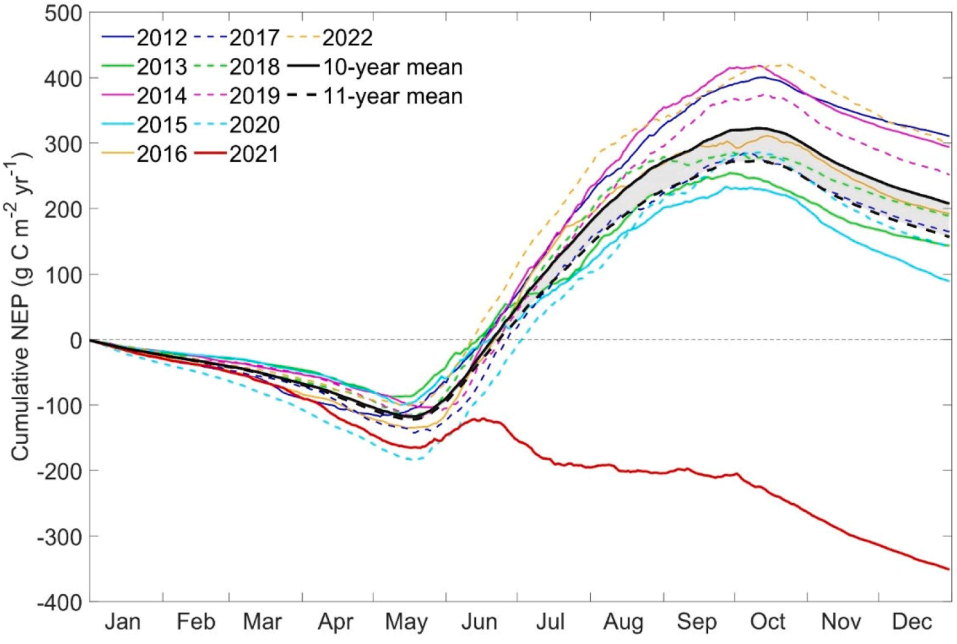

Fig. 8. Daily cumulative net ecosystem productivity (NEP) at TPD from 2012 to 2022. The 10-year mean excludes 2021, while the 11-year mean includes all years. The shaded region illustrates the difference between the two means.

nuclear polyhedrosis virus which would have killed the caterpillar before the pupal stage, hence allowing it to thrive into adulthood (Addy et al., 2018; Hajek et al., 1996; Reilly et al., 2014). It indicates that future changes in precipitation patterns due to climate change might make the fungus, which is a natural control on the infestation, less effective at controlling spongy moth populations in the region (Reilly et al., 2014).

In usual circumstances, warm temperatures and clear skies with high PAR in the spring and summer in 2021 would have resulted in high photosynthesis (GEP) values (Barr et al., 2002). We had observed an increase in photosynthetic capacity in previous years (2019, 2020, and 2022) due to high PAR values. However, in comparison, in 2021, GEP values were lower at the start of the growing season due to warm and dry conditions (Wu et al., 2012; Beamesderfer at al., 2020; Hussain et al., 2024) and they continued to remain low as photosynthesis was limited due spongy moth infestation and the absence of leaves. Given the large increase in below canopy PAR, we can infer that the defoliation of trees allowed greater light penetration into the understory and forest floor, thereby maintaining some degree of photosynthesis (GEP). Similar results were observed in a study by Cook et al. (2008), which examined leaf area following a forest tent caterpillar defoliation in 2001 at a Chequamegon National Forest in north-central Wisconsin, USA. The spongy moth defoliation also reduced competition for understory and trees that were not impacted by spongy moth such as conifers, potentially contributing to enhance GEP (Schäfer et al., 2010). It is likely that the understory and coniferous species present at the site were the dominant contributions to GEP during June and early July. Peak defoliation was reached in early July, after which larvae had transformed into pupae, herbivory seized, and leaves started to re-emerge. A shift (reduction) in below canopy PAR values was observed along with a secondary increase in GEP. This was consistent with the literature which describes a secondary flush of canopy and understory leaves once herbivory by the spongy moth is completed (Clark et al., 2009; Hicke et al., 2012; Stephens et al., 2018; Wiley et al., 2017). This secondary canopy growth is supported by stored carbon pools in tree stems and root tissue but comes at a cost to biomass accumulation (Wiley et al., 2017). Despite a resurgence of secondary leaf growth at our site, GEP remained lower than its pre-infestation average. A study by Wiley et al. (2017) found that black oaks, when defoliated, produced smaller leaves in the secondary flush of foliage, which might explain why GEP did not reach typical values following re-foliage. Schäfer et al. (2010) also discovered that only half of the foliage regrew after a complete defoliation by the spongy moth in the Pine Barrens of New Jersey, USA. Therefore, despite an increase in light penetration and reduced competition, herbivory by spongy moth ultimately results in a decrease in overall ecosystem production (Cook et al., 2008).

In 2021, RE showed an increase of about 11.2 % (136 g C m^{-2}) as compared to mean RE value (1029 ± 139 g C m^{-2}) in non-infestation years at our forest. However, this increase in RE was within interannual variation and is likely the result of several factors. While the spongy moth infestation could be a contributing cause, suitable meteorological conditions during the same time were the likely drivers behind this increase in RE. In the literature both an increase and a decrease in RE have been reported following spongy moth infestations. For example, Cook et al. (2008) reported that respiration rates were 6 % (45 g C m^{-2}) higher following a forest tent caterpillar defoliation in 2001 in north-central Wisconsin, USA. Frost and Hunter (2004) observed an increase in soil respiration following herbivory by the spongy moth in an experiment with red oak saplings. In contrast, Clark et al. (2009) showed a decrease in RE following full stand defoliation by the spongy moth in an Oak/Pine stand. Our forest site, while oak dominated, was not completely defoliated. As mentioned earlier, the understory and conifer trees had leaves, which means foliar and other autotrophic respiration fluxes were still taking place. It is also possible that heterotrophic respiration, which is impacted by soil temperature and soil moisture, could have increased RE (Clark et al., 2009). In fact, we had observed a progressively declining trend in cumulative daily NEP (i.e. RE) prior to the start of the growing season at our site.

An earlier study at our forest site had suggested that RE is predominantly controlled by temperature (Beamesderfer et al., 2020). In 2021, the temperature at our site was among the warmest, accompanied by mid to late summer precipitation events. Therefore, despite the infestation, these environmental factors likely contributed to the observed increase in RE, which, without strong photosynthesis, likely contributed to such a larger observed decrease in NEP in 2021 (i.e. 279 % or −351 - 207±77 g C m^{-2} yr^{-1} change) when compared to mean annual NEP over non-infested years. This marked the first time the forest was a C source in the 11-year study period. In the past, the lowest annual NEP at our site

was observed in 2015. This year experienced comparable meteorological conditions, a similar start to the growing season, and low early growing season precipitation. Despite these environmental conditions, annual GEP in 2015 reached 1346 g C m^{-2} yr^{-1}, as compared to 959 g C m^{-2} yr^{-1} recorded in 2021, while RE was 1282 g C m^{-2} yr^{-1} in 2015 as compared to 1345 g C m^{-2} yr^{-1} in 2021. In 2013, meteorological conditions were also similar to those of 2015, resulting in a decrease in NEP. Additionally in 2020, another year with lower-than-average annual NEP, RE was higher during the early part of the year, more so than in any other year during the study period, leading to an overall reduction in NEP. In all three years 2013, 2015, and 2020 the forest remained a net C sink with an annual NEP value of 89 g C m^{-2} yr^{-1}, 143 g C m^{-2} yr^{-1}, and 142 g C m^{-2} yr^{-1}, respectively. Thus, it is reasonable to assume that, in the absence of the spongy moth defoliation, the forest would have continued to function as a net C sink. Alternatively, in 2012, a hot year similar to 2021, there was a reduction in GEP; however, in this case, both GEP and RE were reduced, resulting in increased NEP. Hence, while the spongy moth appears to play a significant role in the observed decrease in NEP in 2021, it is important to acknowledge the limitations in precisely quantifying the extent of its contribution compared to other factors. Nonetheless, it is notable that no other year exhibits a drop in NEP as observed in 2021. It is also important to note that disturbances generally tend to bolster RE over many years by increasing tree mortality and hence the amount of debris on the forest floor (Renninger et al., 2014). There may also be a lag in time in the decomposition of organic matter following the disturbance as suggested by Renninger et al. (2014), who found that annual RE from snags and coarse woody debris at their site was 3.5 times larger than pre-disturbance levels four years after a spongy moth defoliation. Therefore, it will be interesting to observe long-term impacts of this intense infestation on RE, which may increase in the coming years as a result of potential increase in tree mortality and decomposition of coarse woody debris.

Overall, our study results were consistent with several studies reviewed by Hicke et al. (2012) exploring biotic disturbance impacts on forest C cycling in Canada and USA. Annual NEP of our forest during the disturbance year was very similar to annual NEP of −246 g C m^{-2} yr^{-1} reported by Clark et al. (2018) in a temperate oak stand in New Jersey, USA in 2007.

Temperate forests are an important contributor to the global C sink (Bonan, 2008; Pan et al., 2011; Harris et al., 2021). However, an increase in the intensity and frequency of natural disturbance events, including insect infestations due to climate change can reduce their C sequestration capabilities (Clark et al., 2009; Dale et al., 2001; Hicke et al., 2012; Kurz et al., 2008; Williams et al., 2016), potentially compromising their role in nature-based climate solutions to achieve net zero emission goals (IPCC, 2021). Therefore, it is important to continue efforts to gain a better understanding of forest C exchange processes, exploring potential changes in these processes due to natural disturbances, as well as forest recovery, in order to sustain their C sequestration capabilities.

5. Conclusions

This study assessed the impact of a spongy moth defoliation on a mature oak-dominated temperate forest in the Great Lakes region in Canada, using eddy covariance flux data from 2012 to 2022 and provided quantitative assessment of changes in forest C balance. Overall, the forest was a large C sink with mean annual NEP of 207 ± 77 g C m^{-2} yr^{-1} over non-infestation years. In 2021, GEP declined by approximately 30 % while RE increased by about 12 % as a severe spongy moth infestation caused the forest to become a large source of C with annual NEP of −351 g C m^{-2} yr^{-1}. Study results further showed that optimal meteorological conditions at the start of the growing season as characterized by warm temperature and dry air, likely contributed to the intensity of the outbreak, enabling the moth to thrive in the absence of natural mortality factors. The forest showed a strong recovery in the following year with annual NEP of 298 g C m^{-2} yr^{-1} in 2022. This study provides long-term C flux data including a major transient disturbance event that can be used to further develop ecosystem models and refine forest management practices to improve their resilience to climate change.

Declarations

Ethics approval and consent to participate

Not applicable.

Consent for publication

Not applicable.

Author contributions

LL conducted data analysis, participated in data collection and wrote the first draft of the manuscript. MAA conceptualized the study, secured research grants, established Turkey Point Environmental Observatory Deciduous forest flux tower site (CA-TPD), contributed to data collection and write-up of the manuscript.

CRediT authorship contribution statement

Lejla Latifovic: Writing – review & editing, Writing – original draft, Visualization, Validation, Methodology, Investigation, Formal analysis, Data curation. **M. Altaf Arain:** Writing – review & editing, Writing – original draft, Validation, Supervision, Software, Resources, Project administration, Methodology, Investigation, Funding acquisition, Data curation, Conceptualization.

Declaration of competing interest

The authors declare that they have no known competing financial interests or personal relationships that could have appeared to influence the work reported in this paper.

Data availability

Data will be made available on request.

Funding

This study was funded by the Natural Sciences and Engineering Research Council (NSREC) of Canada Discovery and NSERC Alliance Mission grants, Global Water Futures Program (GWF) Southern Forests Water Futures and GWF Observatory grants and US National Science Foundation (NSF) and Social Science and Humanities Research Council (SSHRC) of Canada funded Global Center for Climate Change Impacts on Transboundary Waters grants awarded to M. Altaf Arain.

Acknowledgments

We thank many researchers and graduate students who helped in data collection and data quality control at this site over the years with special thanks to Jason J. Brodeur, Myroslava Khomik, Robin Thorne, Eric Beamesderfer, Alanna Bodo, Shawn McKenzie, Nur Hussain, Elizabeth Arango Ruda, and Farbod Tabaei. We thank Dave Holmes, Paul Gagnon, and Debbie Thain from Long Point Region Conservation Authority (LPRCA) for their support.

References

Addy, K., Gold, A.J., Loffredo, J.A., Schroth, A.W., Inamdar, S.P., Bowden, et al., 2018. Stream response to an extreme drought-induced defoliation event. Biogeochemistry 140 (2), 199–215. https://doi.org/10.1007/s10533-018-0485-3.

Allaby, M., 2006. Biomes of the Earth: Temperate forests. Chelsea House, New York, NY. ISBN-10: 0816053219, ISBN-13: 9780816053216.

Ammunét, T., Kaukoranta, T., Saikkonen, K., Repo, T., Klemola, T., 2012. Invading and resident defoliators in a changing climate: cold tolerance and predictions concerning extreme winter cold as a range-limiting factor. Ecol. Entomol. 37 (3), 212–220. https://doi.org/10.1111/j.1365-2311.2012.01358.x.

Arain, M.A., 2022. AmeriFlux FLUXNET-1F CA-TPD Ontario - Turkey Point mature deciduous. AmeriFlux (Dataset). doi:10.17190/AMF/1881567.

Arain, M.A., Xu, B., Brodeur, J.J., Khomik, M., Peichl, M., Beamesderfer, E., Restrepo-Couple, N., Thorne, R., 2022. Heat and drought impact on carbon exchange in an age-sequence of temperate pine forests. Ecol. Process. 11 (1), 7. https://doi.org/10.1186/s13717-021-00349-7.

Baldocchi, D.D., 2003. Assessing the eddy covariance technique for evaluating carbon dioxide exchange rates of ecosystems: past, present and future. Glob. Chang. Biol. 9 (4), 479–492. https://doi.org/10.1046/j.1365-2486.2003.00629.x.

Baldocchi, et al., 2001. FLUXNET: A New Tool to Study the Temporal and Spatial Variability of Ecosystem-Scale Carbon Dioxide, Water Vapor, and Energy Flux Densities. Bulletin of the American Meteorological Society, pp. 2415–2434. https://doi.org/10.1175/1520-0477(2001)082<2415:FANTTS>2.3.CO;2.

Barbosa, P., Waldvogel, M., Martinat, P., Douglass, L.W., 1983. Developmental and reproductive performance of the Gypsy Moth, *Lymantria dispar* (L.) (Lepidoptera: lymantriidae), on selected hosts common to Mid-Atlantic and southern forests. Environ. Entomol. 12 (6), 1858–1862. https://doi.org/10.1093/ee/12.6.1858.

Barr, A.G., Griffis, T.J., Black, T.A., Lee, X., Staebler, R.M., Fuentes, J.D., Chen, Z., Morgenstern, K., 2002. Comparing the carbon budgets of boreal and temperate deciduous forest stands. Can. J. Forest Res. 32 (5), 813–822. https://doi.org/10.1139/x01-131.

Beamesderfer, E.R., Arain, M.A., Khomik, M., Brodeur, J.J., 2020. The impact of seasonal and annual climate variations on the carbon uptake capacity of a deciduous forest within the Great Lakes region of Canada. J. Geophys. Res.: Biogeosci. 125 (9) https://doi.org/10.1029/2019JG005389.

Bonan, G.B., 2008. Forests and climate change: forcings, feedbacks, and the climate benefits of forests. Science (1979) 320 (5882), 1444–1449. https://doi.org/10.1126/science.1155121.

Brodeur, J., 2014. Data-driven Approaches For Sustainable Operation and Defensible Results in a long-term, Multi-Site Ecosystem Flux Measurement Program (Doctoral Dissertation). McMaster University, Hamilton, Ontario. Retrieved from MacSphere. http://hdl.handle.net/11375/14091.

Canadell, J.G., Schulze, E.D., 2014. Global potential of biospheric carbon management for climate mitigation. Nat. Commun. 5 (1), 5282. https://doi.org/10.1038/ncomms6282.

Chan, F.C.C., Altaf Arain, M., Khomik, M., Brodeur, J.J., Peichl, M., Restrepo-Coupe, N., et al., 2018. Carbon, water and energy exchange dynamics of a young pine plantation forest during the initial fourteen years of growth. For. Ecol. Manage. 410, 12–26. https://doi.org/10.1016/j.foreco.2017.12.024.

Clark, K., Renninger, H., Skowronski, N., Gallagher, M., Schäfer, K., 2018. Decadal-scale reduction in forest net ecosystem production following insect defoliation contrasts with short-term impacts of prescribed fires. Forests. 9 (3), 145. https://doi.org/10.3390/f9030145.

Clark, K.L., Skowronski, N., Hom, J., 2009. Invasive insects impact forest carbon dynamics. Glob. Chang. Biol. 16 (1), 88–101. https://doi.org/10.1111/j.1365-2486.2009.01983.x.

Commission for Environmental Cooperation, 2006. Ecological Regions of North America: Toward a common Perspective (Original Work Published 1997). Commission for Environmental Cooperation, Montreal, Quebec, Canada. http://www.cec.org.

Cook, B.D., Bolstad, P.V., Martin, J.G., Heinsch, F.A., Davis, K.J., Wang, W., Desai, A.R., Teclaw, R.M., 2008. Using light-use and production efficiency models to predict photosynthesis and net carbon exchange during forest canopy disturbance. Ecosystems 11 (1), 26–44. https://doi.org/10.1007/s10021-007-9105-0.

Coursolle, C., Margolis, H.A., Giasson, M.-A., Bernier, P.-Y., Amiro, B.D., Arain, M.A., et al., 2012. Influence of stand age on the magnitude and seasonality of carbon fluxes in Canadian forests. Agric. For. Meteorol. 165, 136–148. https://doi.org/10.1016/j.agrformet.2012.06.011.

Cullingham, C.I., Cooke, J.E., Dang, S., Davis, C.S., Cooke, B.J., Coltman, D.W., 2011. Mountain pine beetle host-range expansion threatens the boreal forest. Mol. Ecol. 20 (10), 2157–2171. https://doi.org/10.1111/j.1365-294X.2011.05086.x.

Currano, E.D., Wilf, P., Wing, S.L., Labandeira, C.C., Lovelock, E.C., Royer, D.L., 2008. Sharply increased insect herbivory during the Paleocene–Eocene Thermal Maximum. Proceed. Natl. Acad. Sci. 105 (6), 1960–1964. https://doi.org/10.1073/pnas.0708646105.

Crins, W.J., Gray, P.A., Uhlig, P.W.C., Wester, M.C., 2009. The ecosystems of Ontario, part 1: ecozones and ecoregions. Ontario Ministry of Natural Resources, Science & Information Branch, Inventory, Monitoring and Assessment Section. Retrieved from. https://www.ontario.ca/page/ecosystems-ontario-part-1-ecozones-and-ecoregions.

Dale, V.H., Joyce, L.A., Mcnulty, S., Neilson, R.P., Ayres, M.P., Flannigan, et al., 2001. Climate change and forest disturbances. Bioscience 51 (9), 723. https://doi.org/10.1641/0006-3568(2001)051[0723:CCAFD]2.0.CO;2.

Fluxnet-Canada, 2003. Fluxnet-Canada Measurement Protocols.

Frost, C.J., Hunter, M.D., 2004. Insect canopy herbivory and frass deposition affect soil nutrient dynamics and export in oak mesocosms. Ecology 85 (12), 3335–3347. https://doi.org/10.1890/04-0003.

Harris, N.L., Gibbs, D.A., Baccini, A., Birdsey, R.A., De Bruin, S., Farina, M., et al., 2021. Global maps of twenty-first century forest carbon fluxes. Nat. Clim. Chang. 11 (3), 234–240. https://doi.org/10.1038/s41558-020-00976-6.

Hajek, A.E., Elkinton, S., Witcosky, J., 1996. Introduction and spread of the fungal pathogen *Entomophaga maimaiga* (Zygomycetes: entomophthorales) along the leading edge of Gypsy Moth (Lepidoptera: lymantriidae) spread. Environ. Entomol. 25 (5), 1235–1247. https://doi.org/10.1093/ee/25.5.1235.

Hicke, J.A., Allen, C.D., Desai, A.R., Dietze, M.C., Hall, R.J., Hogg, E.H., et al., 2012. Effects of biotic disturbances on forest carbon cycling in the United States and Canada. Glob. Chang. Biol. 18 (1), 7–34. https://doi.org/10.1111/j.1365-2486.2011.02543.x.

Hicke, J.A., Meddens, A.J.H., Allen, C.D., Kolden, C.A., 2013. Carbon stocks of trees killed by bark beetles and wildfire in the western United States. Environ. Res. Lett. 8 (3) https://doi.org/10.1088/1748-9326/8/3/035032.

Hicke, J.A., Xu, B., Meddens, A.J.H., Egan, J.M., 2020. Characterizing recent bark beetle-caused tree mortality in the western United States from aerial surveys. For. Ecol. Manage. 475, 118402 https://doi.org/10.1016/j.foreco.2020.118402.

Hussain, N., Gonsamo, A., Wang, S., Arain, M.A., 2024. Assessment of spongy moth infestation impacts on forest productivity and carbon loss using the Sentinel-2 satellite remote sensing and eddy covariance flux data. Ecol. Process. 13, 37 https://doi.org/10.1186/s13717-024-00520-w.

Hurteau, M.D., 2021. The role of forests in the carbon cycle and in climate change. In: Letcher, T.M. (Ed.), Climate Change, 3rd Edition. Elsevier B.V, pp. 561–579. https://doi.org/10.1016/B978-0-12-821575-3.00027-X.

IPCC, 2014. Terrestrial and inland water systems. In: Field, C.B., et al. (Eds.), Climate Change 2014: Impacts, adaptation, and vulnerability. Part A: Global and Sectoral aspects. Contribution of Working Group II to the Fifth Assessment Report of the Intergovernmental Panel On Climate Change. Cambridge University Press, Cambridge, United Kingdom and New York, NY, USA, pp. 271–359. https://www.ipcc.ch/site/assets/uploads/2018/02/WGIIAR5-Chap4_FINAL.pdf.

IPCC, 2021. In: Masson-Delmotte, V., et al. (Eds.), Climate Change 2021: The physical Science basis. Contribution of Working Group I to the Sixth Assessment Report of the Intergovernmental Panel On Climate Change. Cambridge University Press, Cambridge, United Kingdom and New York, NY, USA. https://doi.org/10.1017/9781009157896.

Keenan, T.F., Williams, C.A., 2018. The terrestrial carbon sink. Annu Rev. Environ. Resour. 43 (1), 219–243. https://doi.org/10.1146/annurev-environ-102017-030204.

Kurz, W.A., Dymond, C.C., Stinson, G., Rampley, G.J., Neilson, E.T., Carroll, A.L., Ebata, T., Safranyik, L., 2008. Mountain pine beetle and forest carbon feedback to climate change. Nature 452 (7190), 987–990. https://doi.org/10.1038/nature06777.

Leonard, D.E., 1981. Chapter 2: bioecology of the Gypsy Moth. In: Doane, C.C., McManus, M.L. (Eds.), The Gypsy Moth: Research toward Integrated Pest Management. U. S. Department of Agriculture, Washington, DC, pp. 9–29. Retrieved from. https://handle.nal.usda.gov/10113/CAT82474520.

Leroy, B.M.L., Lemme, H., Braumiller, P., Hilmers, T., Jacobs, M., Hochrein, S., et al., 2021. Relative impacts of gypsy moth outbreaks and insecticide treatments on forest resources and ecosystems: an experimental approach. Ecolog. Solut. Evid. 2 (1) https://doi.org/10.1002/2688-8319.12045.

Li, Y., Zhang, W., Schwalm, C.R., Gentine, P., Smith, W.K., Ciais, P., et al., 2023. Widespread spring phenology effects on drought recovery of northern hemisphere ecosystems. Nat. Clim. Chang. 13 (2), 182–188. https://doi.org/10.1038/s41558-022-01584-2.

Liebhold, A.M., Halverson, J.A., Elmes, G.A., 1992. Gypsy Moth invasion in North America: a quantitative analysis. J. Biogeogr. 19 (5), 513. https://doi.org/10.2307/2845770.

Lindroth, R.L., Klein, K.A., Hemming, J.D.C., Feuker, A.M., 1997. Variation in temperature and dietary nitrogen affect performance of the gypsy moth (Lymantria dispar L.). Physiol. Entomol. 22 (1), 55–64. https://doi.org/10.1111/j.1365-3032.1997.tb01140.x.

Lovett, G.M., Cole, J.J., Pace, M.L., 2006. Is net ecosystem production equal to ecosystem carbon accumulation? Ecosystems 9, 152–155. https://doi.org/10.1007/s10021-005-0036-3.

Monson, R.K., 2014. Ecology of temperate forests. In: Monson, R.K., Tester, M., Jorgensen, R. (Eds.), Ecology and the Environment. The Plant Sciences. Springer, New York, NY, pp. 273–296. https://doi.org/10.1007/978-1-4614-7501-9_5. Vol 8.

Ontario Ministry of Northern Development, Mines, Natural Resources and Forestry, 2021. Forest Health Conditions in Ontario 2021. Science and Research Branch. https://www.ontario.ca/page/forest-health-conditions. ISBN 978-1-4868-5876-7.

Pan, Y., Birdsey, R.A., Fang, J., Houghton, R., Kauppi, P.E., Kurz, W.A., et al., 2011. A large and persistent carbon sink in the world's forests. Science (1979) 333 (6045), 988–993. https://doi.org/10.1126/science.1201609.

Pernek, M., Pilas, I., Vrbek, B., Benko, M., Hrasovec, B., Milkovic, J., 2008. Forecasting the impact of the Gypsy moth on lowland hardwood forests by analyzing the cyclical pattern of population and climate data series. For. Ecol. Manage. 255 (5–6), 1740–1748. https://doi.org/10.1016/j.foreco.2007.11.031.

Presant, E.W., Acton, C.J., 1984. Report no. 57. Ontario Institute of Pedology, Ontario Ministry of Agriculture and Food. Vol 2 Retrieved from. https://www.worldcat.org/title/soils-of-the-regionalmunicipality-of-haldimand-norfolk/oclc/630077090.

Régnière, J., Nealis, V., Porter, K., 2009. Climate suitability and management of the gypsy moth invasion into Canada. Biol. Invasions 11 (1), 135–148. https://doi.org/10.1007/s10530-008-9325-z.

Reilly, J.R., Hajek, A.E., Liebhold, A.M., Plymale, R., 2014. Impact of Entomophaga maimaiga (Entomophthorales: entomophthoraceae) on outbreak Gypsy Moth

populations (Lepidoptera: erebidae): the role of weather. Environ. Entomol. 43 (3), 632–641. https://doi.org/10.1603/EN13194.
Reinmann, A.B., Susser, J.R., Demaria, E.M.C., Templer, P.H., 2019. Declines in northern forest tree growth following snowpack decline and soil freezing. Glob. Chang. Biol. 25 (2), 420–430. https://doi.org/10.1111/gcb.14420.
Renninger, H.J., Carlo, N., Clark, K.L., Schäfer, K.V.R., 2014. Modeling respiration from snags and coarse woody debris before and after an invasive gypsy moth disturbance. J. Geophys. Res.: Biogeosci. 119 (4), 630–644. https://doi.org/10.1002/2013JG002542.
Richart, M., Hewitt, N., 2008. Forest Remnants in the Long Point Region, Southern Ontario: tree species diversity and size structure. Landsc. Urban. Plan. 86 (1), 25–37. https://doi.org/10.1016/j.landurbplan.2007.12.005.
Rogers, C., Chen, J.M., Croft, H., Gonsamo, A., Luo, X., Bartlett, P., Staebler, R.M., 2021. Daily leaf area index from photosynthetically active radiation for long term records of canopy structure and leaf phenology. Agric. For. Meteorol. 304–305, 108407 https://doi.org/10.1016/j.agrformet.2021.108407.
Sambaraju, K.R., Carroll, A.L., Aukema, B.H., 2019. Multiyear weather anomalies associated with range shifts by the mountain pine beetle preceding large epidemics. For. Ecol. Manage. 438, 86–95. https://doi.org/10.1016/j.foreco.2019.02.011.
Schäfer, K.V.R., Clark, K.L., Skowronski, N., Hamerlynck, E.P., 2010. Impact of insect defoliation on forest carbon balance as assessed with a canopy assimilation model. Glob. Chang. Biol. 16 (2), 546–560. https://doi.org/10.1111/j.1365-2486.2009.02037.x.
Speckman, H.N., Frank, J.M., Bradford, J.B., Miles, B.L., Massman, W.J., Parton, W.J., Ryan, M.G., 2015. Forest ecosystem respiration estimated from eddy covariance and chamber measurements under high turbulence and substantial tree mortality from bark beetles. Glob. Chang. Biol. 21 (2), 708–721. https://doi.org/10.1111/gcb.12731.
Stephens, J.J., Black, T.A., Jassal, R.S., Nesic, Z., Grant, N.J., Barr, A.G., et al., 2018. Effects of forest tent caterpillar defoliation on carbon and water fluxes in a boreal aspen stand. Agric. For. Meteorol. 253–254, 176–189. https://doi.org/10.1016/j.agrformet.2018.01.035.
Tyrrell, M.L., Ross, J., Kelty, M, 2012. Carbon dynamics in the temperate forest. In: Ashton, M.S., Tyrrell, M.L., Spalding, D., Gentry, B. (Eds.), Managing Forest Carbon in a Changing Climate. Springer Science & Business Media, Dordrecht, Netherlands, pp. 77–107. https://doi.org/10.1007/978-94-007-2232-3_5.
United States Department of Agriculture, Forest Services, Eastern Region State and Private Forestry, 2022. Eastern Region Forest Health Conditions Report 2021. Retrieved from. https://www.fs.usda.gov/foresthealth/publications/fhp/index.shtml.
Vasseur, L., 2012. Restoration of deciduous forests. Nat. Educ. Knowl. 3 (12), 1.
Ward, J.S., Jones, C.C., Barsky, J.P., 2022. Multiyear defoliations in southern New England increases oak mortality. Can. J. For. Res. 52 (2), 269–279. https://doi.org/10.1139/cjfr-2021-0174.
Waring, B., Neumann, M., Prentice, I.C., Adams, M., Smith, P., Siegert, M., 2020. Forests and decarbonization – Roles of natural and planted forests. Front. For. Glob. Change 3. https://doi.org/10.3389/ffgc.2020.00058.
Weed, A.S., Ayres, M.P., Hicke, J.A., 2013. Consequences of climate change for biotic disturbances in North American forests. Ecol. Monogr. 83 (4), 441–470. https://doi.org/10.1890/13-0160.1.
Wiley, E., Casper, B.B., Helliker, B.R., 2017. Recovery following defoliation involves shifts in allocation that favour storage and reproduction over radial growth in black oak. J. Ecol. 105 (2), 412–424. https://doi.org/10.1111/1365-2745.12672.
Williams, C.A., Gu, H., MacLean, R., Masek, J.G., Collatz, G.J., 2016. Disturbance and the carbon balance of US forests: a quantitative review of impacts from harvests, fires, insects, and droughts. Glob. Planet. Change 143, 66–80. https://doi.org/10.1016/j.gloplacha.2016.06.002.
Wu, J., van der Linden, L., Lasslop, G., Carvalhais, N., Pilegaard, K., Beier, C., Ibrom, A., 2012. Effects of climate variability and functional changes on the interannual variation of the carbon balance in a temperate deciduous forest. Biogeosciences 9 (1), 13–28. https://doi.org/10.5194/bg-9-13-2012.